Oil & Gas Science and Technology - Rev. IFP Energies nouvelles **74**, 11 (2019)

https://doi.org/10.2516/ogst/2018084

Available online at:
ogst.ifpenergiesnouvelles.fr

REGULAR ARTICLE OPEN ACCESS

Formation damage due to asphaltene precipitation during CO_2 flooding processes with NMR technique

Kun Qian[1], Shenglai Yang[1,*], Hong-en Dou[2], Jieqiong Pang[1], and Yu Huang[1]

[1] State Key Lab of Oil and Gas Resources and Engineering, China University of Petroleum-Beijing, Beijing 102249, People's Republic of China
[2] Research Institute of Petroleum Exploration and Development, CNPC, Beijing 100083, People's Republic of China

Received: 17 July 2018 / Accepted: 5 November 2018

Abstract. In order to quantitatively evaluate the pore-scale formation damage of tight sandstones caused by asphaltene precipitation during CO_2 flooding, the coreflood tests and Nuclear Magnetic Resonance (NMR) relaxometry measurements have been designed and applied. Five CO_2 coreflood tests at immiscible, near-miscible and miscible conditions were conducted and the characteristics of the produced oil and gas were analyzed. For each coreflood test, the T_2 spectrum of the core sample was measured and compared before and after CO_2 flooding to determine the asphaltene precipitation distribution in pores. It is found that, the solubility and extraction effect of the CO_2 plays a more dominant role in the CO_2-EOR (Enhanced Oil Recovery) process with higher injection pressure. And, more light components are extracted and recovered by the CO_2 and more heavy components including asphaltene are left in the core sample. Thus, the severity of formation damage influenced by asphaltene precipitation increases as the injection pressure increases. In comparison to micro and small pores (0.1–10 ms), the asphaltene precipitation has a greater influence on the medium and large pores (10–1000 ms) due to the sufficient interaction between the CO_2 and crude oil in the medium and large pores. Furthermore, the asphaltene precipitation not only causes pore clogging, but also induces rock wettability to alter towards oil-wet direction.

1 Introduction

CO_2 flooding has been proven to be an effective technique to Enhanced Oil Recovery (EOR) through both laboratory experiments and field application for several decades [1–3]. The injected CO_2 could interact with crude oil in the reservoirs, leading to significant effects on EOR. The main mechanisms of CO_2-EOR technique include oil-swelling effect, viscosity reduction, light-hydrocarbon extraction and interfacial tension reduction [4]. However, it has been reported that the interaction between CO_2 and crude oil is the determine factor for asphaltene precipitation. For example, in Midale in Canada, no prior asphaltene problem was encountered until CO_2 injection. Asphaltene precipitation also occurred in other CO_2 floods, such as in Little Creek Field, Mississippi and West Texas [5].

Asphaltene precipitation could cause serious damages to formations [5–7]. This is because the precipitated asphaltene will deposit on to the reservoir rocks, which may cause reservoir plugging and wettability alteration [8, 9]. To investigate asphaltene precipitation during CO_2 flooding processes, extensive coreflood experimental studies have been conducted. Wang *et al.* [10] found that the degree of permeability reduction is positively correlated with the percentage of asphaltene precipitated through CO_2 core flooding tests. Cao and Gu [11] demonstrated that less amount of asphaltene remained in the cores in immiscible conditions while more asphaltene precipitation is observed under miscible conditions. Wang *et al.* [12] found that permeability reduction due to asphaltene precipitation mainly occurs in the middle and tail end of the reservoir in the miscible CO_2 Water-Alternating-Gas (WAG) injection after the continuous CO_2 injection through long coreflood experiments. Moreover, the wettability alteration also occurs due to asphaltene precipitation, which has negative influence on the formation. Amroun and Tiab [13] and Escrochi *et al.* [14] reported that the asphaltene precipitation was the main platform for wettability alteration and the porous media changed towards strongly oil-wet condition. Uetani [15] reported that the productivity dropped immediately and water cut increased from 2–3% to 10–15% in field "M", which was caused by the rock wettability altered form water-wet to oil-wet because of asphaltene precipitation.

Although, the asphaltene precipitation during CO_2 flooding could be determined through the measurement of

* Corresponding author: yangshenglai_cupb@126.com

permeability reduction combined with the asphaltene content of the produced oil [16, 17]. The pore-scale distribution of asphaltene deposition has been rarely investigated. Srivastava *et al.* [18] used X-ray CAT (Computer Aided Tomography)-scanning technique to visualize the asphaltene deposition along the length of the core. Song *et al.* [19] made a microscopic model to observe the distribution of asphaltene deposition in 2-D porous networks. However, these methods can only qualitatively observe the distribution of asphaltene precipitation, and the influence of asphaltene precipitation on the pores cannot be quantitatively evaluated. In order to quantitatively analyze the distribution of asphaltene precipitation in pores, Wang *et al.* [10] applied Nuclear Magnetic Resonance (NMR) to scan tight artificial cores before and after CO_2 flooding. Besides determining the distribution of asphaltene precipitation, NMR technique is a powerful tool for non-invasively analyzing the wetting state of rock [20, 21]. Shikhov *et al.* [22] studied the wettability change of sandstone cores over aging time with low-field NMR measurements.

In this study, an analysis method reference to Amott method [23] was proposed to quantitatively evaluate the wettability alteration before and after CO_2 flooding combined with determining the distribution of asphaltene precipitation. First, in order to determine the influence of CO_2-brine-rock interaction on the core samples, two core samples saturated with kerosene which does not contain asphaltene were applied to conduct CO_2 coreflood experiments. Then, five CO_2 coreflood tests were conducted at different injection pressures. The oil recovery factors, the viscosity and the asphaltene contents of the produced oil were measured during these tests. Then, through comparing the difference in the NMR transverse relaxation time (T_2) spectrum for the water-saturated cores before and after CO_2 flooding, the distribution of asphaltene precipitation in the pores and throats of core samples was quantitatively evaluated. At the same time, the wettability alteration condition was evaluated by calculating the condition of oil saturation in pores before and after CO_2 flooding. On these bases, this study can help to improve the system of quantitatively evaluating the distribution of the asphaltene precipitation and wettability alteration in pores and throats.

2 Experimental section

2.1 Materials

In this study, the Stock Tank Oil (STO) sample was collected from Changqing Oilfield, China. The density and viscosity of the cleaned STO were measured to be 833.4 kg/m^3 and 4.76 mPa s at the atmospheric pressure and 61 °C and the MW_{oil} = 229.7 g/mol. The asphaltene content of the cleaned crude oil was measured to be 0.94 wt% (*n*-pentane insoluble) with the standard ASTM D2007-03 method [24]. The wax content was measured by the Thin-Layer Chromatograph/Flame Ionization Detection (TLC-FID) method and the Saturate, Aromatic, Resin and Asphaltene (SARA) analysis of the crude oil was measured with the standard SATM D4124, as shown in Table 1. The density and viscosity of the kerosene were measured to be 792.0 kg/m^3 and 1.01 mPa s at the atmospheric pressure and 61 °C. The Gas Chromatography (GC) compositional analysis of the cleaned crude oil sample and kerosene is given in Table 2.

The reservoir brine sample was collected from the same formation and cleaned. The reservoir brine has the Total Dissolved Solids (TDS) of 30 917.8 mg/L, which was considered to be the water type of calcium chloride. The brine viscosity was measured to be 0.4 mPa s at the atmospheric pressure and 61 °C. The purity of the CO_2 used in this study was equal to 99.99% supplied by *Beijing Huayuan Gas Chemical Co. Ltd.*

Table 1. Wax content and SARA analysis of the crude oil.

Component	Weight percent (wt%)
Wax	0.10
Saturates	66.63
Aromatics	27.54
Resins	4.89
Asphaltenes	0.94

Table 2. Compositional analysis of the crude oil with the asphaltene content of w_{asp} = 0.94 wt% (*n*-pentane insoluble) and the kerosene without asphaltene.

Carbon no.	mol%		Carbon no.	mol%	
	Crude oil	Kerosene		Crude oil	Kerosene
C_1			C_{19}	1.90	
C_2			C_{20}	1.22	
C_3	0.33		C_{21}	1.13	
C_4	3.82		C_{22}	0.99	
C_5	6.46	0.54	C_{23}	0.94	
C_6	7.05	0.69	C_{24}	0.78	
C_7	10.62	2.32	C_{25}	0.71	
C_8	9.90	8.84	C_{26}	0.67	
C_9	8.49	28.36	C_{27}	0.63	
C_{10}	6.82	38.78	C_{28}	0.63	
C_{11}	5.73	14.23	C_{29}	0.51	
C_{12}	4.34	2.52	C_{30}	0.54	
C_{13}	3.49	0.96	C_{31}	0.58	
C_{14}	3.64	0.71	C_{32}	0.49	
C_{15}	3.26	0.60	C_{33}	0.36	
C_{16}	2.60	0.52	C_{34}	0.28	
C_{17}	2.33	0.51	C_{35}	0.44	
C_{18}	2.17	0.40	C_{36+}	6.04	
			Total	100.00	100.00

2.2 MMP tests

Figure 1 shows the schematic diagram of the slim-tube apparatus (CFS-100, *Core Lab, Tulsa, OK, USA*) for conducting a series of displacement experiments to determine the Minimum Miscibility Pressure (MMP) of the crude oil – CO_2 system in this study. The apparatus was consisted of a displacement pump (260D, *ISCO, Lincoln, NE, USA*), a stainless steel slim tube packed with silica sands (*Shengfa Mining Industry Co. Ltd., China*), a back-pressure regulator (*Huada, Haian, China*) and two pressure transducers to monitor injection pressure and back pressure constantly. A burette was used to collect and measure the produced oil and a gas flow meter to measure the volume of the produced gas.

In this study, the MMP of the CO_2-crude oil system was determined by six slim-tube tests with different injection pressure at the formation temperature of 61 °C. The displacement system was cleaned by petroleum ether and dried by nitrogen several times in preparation of each slim-tube tests. Then, the apparatus was saturated with the crude oil at the reservoir temperature of $T_{res} = 61$ °C with a constant flow rate of 0.2 cm^3/min and the back pressure should be maintained the desired production pressure in order to prevent the crude oil from degassing. The CO_2 was injected into the slim tube to displace the crude oil with a constant flow rate of 0.1 cm^3/min at the set injection pressure. The injection and production pressure was continuously monitored and recorded during the entire experiment. The volume of the produced oil and gas was measured at every 0.1 PV of pure CO_2 until 1.2 PV CO_2 was injected.

2.3 Coreflood tests

Figure 2 depicts the schematic diagram of the high-pressure coreflood apparatus used for CO_2 coreflood tests. A constant flow pump (260D, *ISCO, Lincoln, NE, USA*) was applied to displace dead crude oil, brine and CO_2 through the core plug inside a high-pressure stainless steel coreholder (*Huada, Haian, China*) with the inner diameter and outer diameter of 25 mm and 40 mm. Three high pressure cylinders were applied to store and deliver crude oil, brine and CO_2, respectively. Another *ISCO* syringe pump was used to exert the confining pressure which was always kept 2–3 MPa higher than the injection pressure on the core plug. All above mentioned components were placed inside an air bath which was heated by two electronic heat guns. A temperature controller was used to keep the air bath at the reservoir temperature of 61 °C. A back-pressure regulator (*Huada, Haian, China*) was used to target the desired production pressure during the coreflood test. A burette was used to collect and measure the produced oil and a gas flow meter to measure the volume of the produced gas.

The core samples used in this experiment are tight cores collected from Changqing Oil Field, China. It is noted that the core samples with nearly the same gas permeability pore size distribution are selected, which are from the same formation. The properties of cores are listed in Table 3.

The general procedure for the CO_2 coreflood tests is briefly described as follows:

1. Prior to each test, the core plugs were thoroughly cleaned by using a Dean−Stark extractor (SXT-02, *Shanghai Ping Xuan Scientific Instrument Co., Ltd., China*) for 20–30 days. After the core plugs were cleaned and dried at 100 °C. The gas permeability and porosity were measured with nitrogen (High-Pressure Gas Permeameter/Porosimeter, *Temco, Tulsa, OK, USA*).
2. The core plug was placed in the high-pressure coreholder and vacuumed for 24 hours. Then the formation brine was injected at the flow rate of 0.2 cm^3/min to saturate the core plug. Then, the NMR apparatus was used to measure T_2 transverse relaxation time of the core sample under initial water-saturated condition.
3. The core was displaced with the $MnCl_2$ solution (15 000 mg/L) of 5 PV. And then the saturated core was scanned again by NMR apparatus to make sure the hydrogen signal of the brine eliminated.
4. After that, 3.0 PV of the crude oil was pumped through the core plugs at a constant rate of 0.1 cm^3/min until no water was produced to achieve the connate water saturation (S_{wc}) the initial oil saturation (S_{oi}) at the reservoir temperature of 61 °C. The physical properties of core plugs were listed in Table 3. The T_2 spectrum was measured again after the core had been saturated with crude oil.
5. In each test, 2.0 PV CO_2 was pumped into the coreholder to displace the crude oil at the desired injection pressure and reservoir temperature of 61 °C. The injection and production pressure was continuously monitored and recorded during the entire test. The cumulative produced oil volume was recorded by a video camera and the cumulative volume of the produced gas was measured and recorded by using the gas flow meter. The produced oil and gas were collected during each coreflood test and the components of the produced oil and gas were analyzed by GC technique.
6. After the CO_2 coreflood test, the core samples, were cleaned by a Soxhlet Extractor with the solvent of petroleum ether which cannot dissolve asphaltene [25] and dried for 12 h at 100 °C. The gas permeability core samples were measured by permeameter with nitrogen.
7. The cleaned core sample was conducted the same treatments from step 1 to step 4.

2.4 NMR tests

NMR refers to the response of atomic nuclei to magnetic fields. The NMR apparatus (Mini-MR, *Niumag, Suzhou, China*) used in this study detects the transverse relaxation motion of ^1H of fluids in the pores, which produces a relatively strong signal compared to other elements in earth formations [26]. The magnetic intensity, gradient value control precision and frequency range of the NMR apparatus are

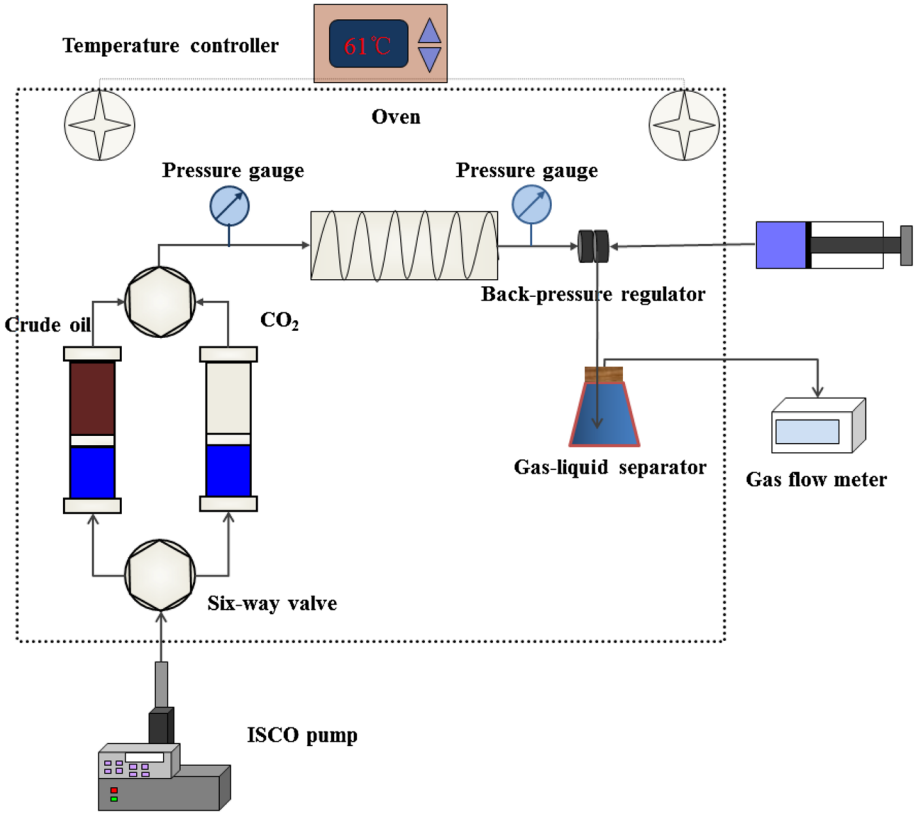

Fig. 1. Schematic diagram of the slim-tube test setup.

0.5 T, 0.025 T/m, 0.01 MHz and 1–30 MHz, respectively. As for the NMR transverse relaxation time of fluid in the pore is given as [27, 28]:

$$\frac{1}{T_2} = \frac{1}{T_{2S}} + \frac{1}{T_{2D}} + \frac{1}{T_{2B}}. \quad (1)$$

T_{2S}: the surface relaxation time (ms);
T_{2D}: the relaxation time as induce by diffusion in magnetic gradients (ms);
T_{2B}: the bulk relaxation time of the pore-filling fluid (ms).

Because T_{2B} is much larger than T_2 for fluid in porous media, T_{2B} is usually neglected. T_{2D} is reasonably neglected, when the magnetic field is thought to be uniform with a quite small field gradient and echo time is small enough. Furthermore, T_{2S} is associated with specific surface of a pore. Then,

$$\frac{1}{T_2} \approx \frac{1}{T_{2S}} = \rho_2 \left(\frac{S}{V}\right), \quad (2)$$

ρ_2: the surface relaxation rate (um/ms);
S: the interstitial surface area (um_2);
V: the pore volume (um_3).

S/V can be written as a function of the dimensionless shape factor of a pore, F_S, and pore radius, r (um), as follows,

$$\frac{S}{V} = \frac{F_S}{r}. \quad (3)$$

Combining equations (2) and (3),

$$T_2 = \frac{1}{\rho_{2F_S}} r, \quad (4)$$

then,

$$T_2 = Cr, \quad (5)$$

$$C = \frac{1}{\rho_{2F_S}}, \quad (6)$$

C is considered to be a constant for equations (5) and (6) so the T_2 response is proportional to the pore radius. In our work, 0.1–1 ms of T_2 is defined as micro pores, 1–10 ms defined as small pores, 10–100 ms defined as medium pores and 100–1000 ms as large pores.

3 Results and discussion

3.1 Experimental identification of CO_2/brine/rock interactions with NMR technique

In the CO_2 flooding process, the solid precipitation was partly generated due to CO_2/bine/rock reactions. The solid

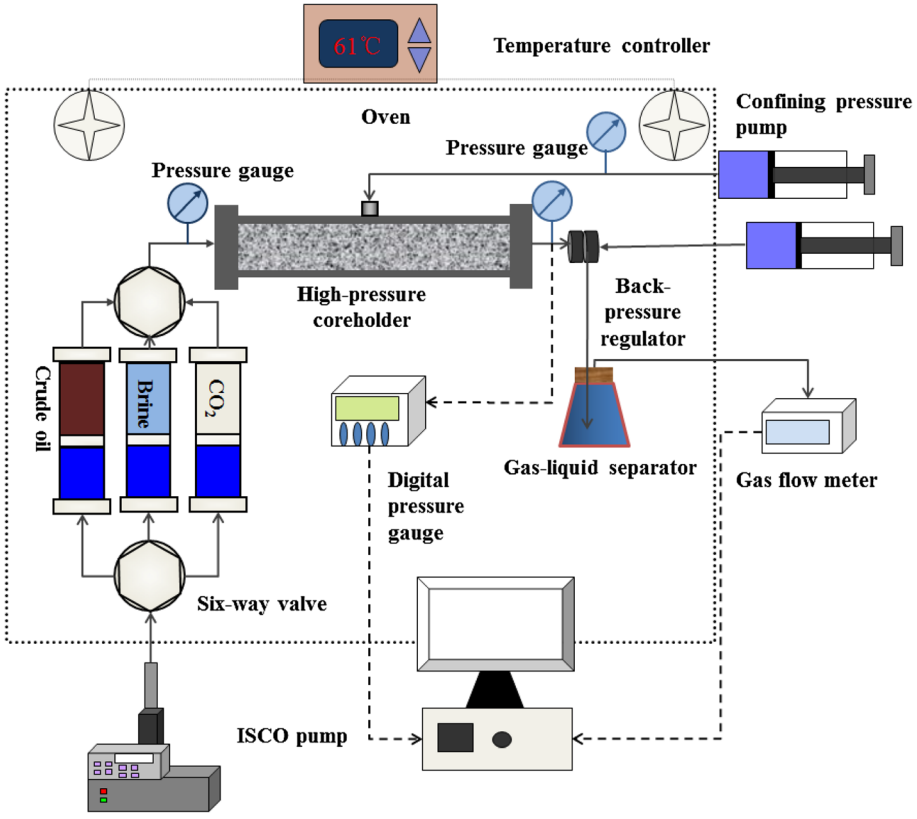

Fig. 2. Schematic diagram of the high-pressure CO_2 coreflood apparatus.

Table 3. Basic properties of tight core plug samples.

No.	Length (cm)	Diameter (cm)	k (mD)	φ (%)	Saturated oil	S_{oi} (%)	S_{wc} (%)
1–1	5.872	2.504	2.67	16.74	Kerosene	67.58	32.42
1–2	6.370	2.504	3.23	17.35		74.41	25.59
2–1	5.126	2.504	2.61	16.23	Crude oil	66.71	33.29
2–2	6.722	2.504	2.91	17.27		68.30	31.70
2–3	5.874	2.504	2.98	16.18		62.75	37.25
2–4	5.660	2.504	3.14	17.94		65.24	34.76
2–5	5.938	2.504	3.31	17.07		70.93	29.07

k: gas porosity of the core plugs;
φ: absolutely gas permeability of the core plugs;
S_{oi}: initial oil saturation;
S_{wc}: initial connate water saturation.

precipitation and clay particles would migrate in the pore and possibly cause a blockage in the pore throat [29]. So that, the CO_2/bine/rock reactions would induced permeability reduction of the cores [30]. Nevertheless the studies on the permeability reduction due to CO_2/bine/rock reactions are basically about aquifers. It is necessary to investigate the influence of the CO_2/bine/rock reactions on permeability reduction of oil reservoir formation before the experimental study on the impact of asphaltene precipitation on permeability. Therefore, instead the crude oil, the kerosene without asphaltene was used to conduct the coreflood experiments first.

As shown in Figure 3, the T_2 spectrum for the initial water-saturated cores 1–1 and 1–2, and the T_2 spectrum for the water-saturated cores after CO_2 flooding, were measured. It can been seen from Figures 3a and 3b that the T_2 spectrum for the water-saturated core after CO_2 flooding did not deviate from the T_2 spectrum for the initial water-saturated cores. Thus, in the case of experimental error, the distribution of pores was considered unchanged. The

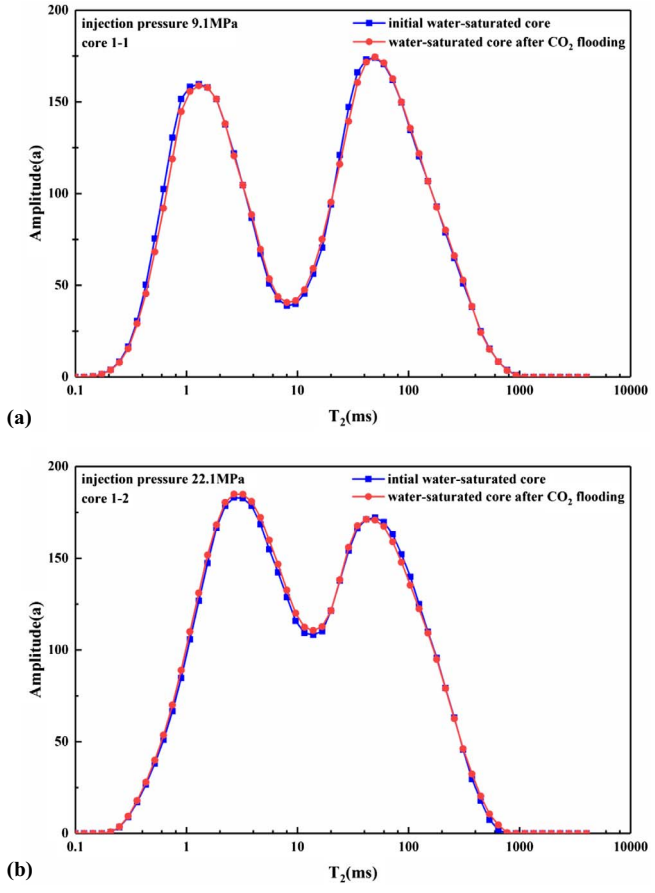

Fig. 3. Comparison of T_2 spectrum for the initial water-saturated cores and for the water-saturated cores after CO_2 flooding and cleaning.

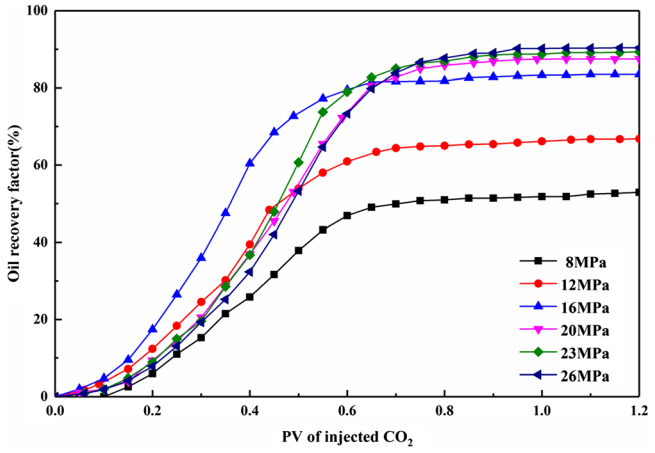

Fig. 4. Oil recovery factors *versus* volume of the injected CO_2 in terms of the PV at injection pressure from 8–26 MPa and a temperature of 61 °C in slim-tube tests.

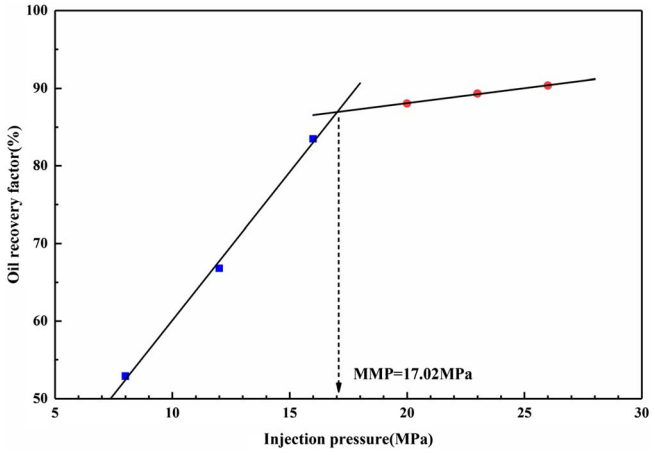

Fig. 5. Variation of the cumulative oil recovery factor determined at 1.2 PV of injected CO_2 at different injection pressures.

experimental result is different from similar experimental results in other literature that the CO_2/bine/rock reactions occur and change the pore structure in the cores during CO_2 coreflood tests [31, 32]. That is because that the reaction time of these coreflood tests is too short in comparison with experiments in other literature. Therefore, the CO_2/bine/rock reactions are considered to have no influence on the pore distribution of the sandstone cores saturated with oil during the CO_2 flooding process.

3.2 CO_2-oil MMP

In this study, the slim-tube tests at six different injection pressures under a constant reservoir temperature of 61 °C were conducted to determine the MMP of the crude oil sample. The measured Oil Recovery Factors (ORF) *versus* Pore Volume (PV) of injected were illustrated in Figure 4. As expected, the ORF increased with the injection of CO_2 at each injection pressure, and the growth rate of the ORFs decreased rapidly after 0.6 PV of injected CO_2 because of the CO_2 breakthrough. There was no more oil obtained in each test at 1.2 PV of injected CO_2 which was the terminal point. Because the rate of CO_2 extraction and dissolution accelerated with the growth of injection pressure [16], leading to stronger swelling effect and lower capillary resistance. The ultimate ORF of each slim-tube test increased as the injection pressure increased. In addition, the ultimate ORF at $P_{inj} = 20$ MPa, 23 MPa and 26 MPa have no obvious growth, which indicates that the MMP measured by slim-tube test is between 16 MPa $\leq P_{inj} \leq$ 20 MPa. After that, the ultimate ORFs of each slim-tube test *versus* injection pressure were depicted in Figure 5 to determine the MMP. Figure 5 shows that the first three points and the last three points are linear respectively. The intersection point of two fitting curves is regarded as the MMP of the CO_2-crude oil system measured by slim-tube test, which is 17.02 MPa.

3.3 Physicochemical characterization of produced fluids

Figure 6 shows the measured ORF *versus* PV of injected CO_2 at different injection pressures of five coreflood tests

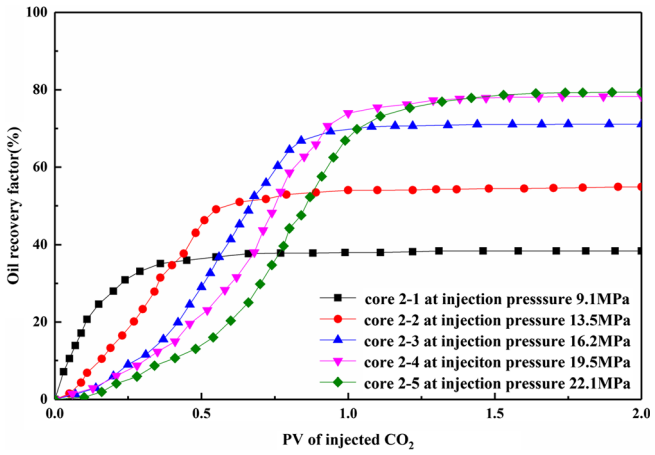

Fig. 6. Oil recovery factors *versus* PV of the injected CO_2 at different injection pressures.

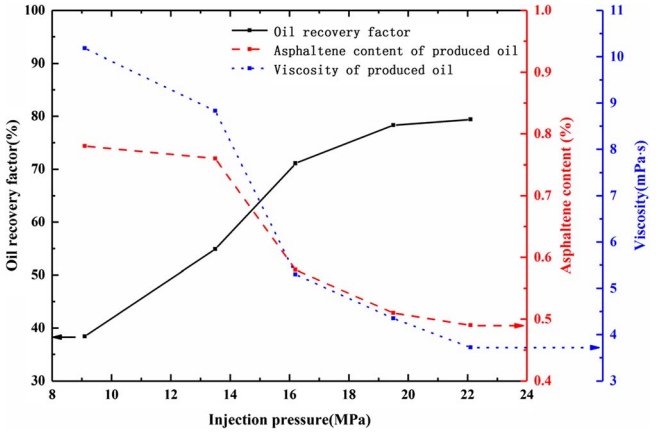

Fig. 7. Oil recovery factor, asphaltene content of CO_2-pruduced oil and viscosity of produced oil *versus* the injection pressure of each coreflood test at the temperature of 61 °C.

under the reservoir temperature of 61 °C. As expected, the ORF increased with the injection of the CO_2 until no more oil was produced at 2.0 PV of injected CO_2. And, the ORFs increased faster before the injected CO_2 of 0.30 PV, 0.55 PV, 0.85 PV, 1.00 PV and 1.10 PV corresponding to the injection pressure of P_{inj} = 9.1 MPa, 13.5 MPa, 16.2 MPa, 19.5 MPa and 22.1 MPa, respectively. More specifically, the ORF of lower injection pressure was greater than that of higher injection pressure in the initial period of process. Because a less portion of injected CO_2 was dissolved into the light crude oil at a lower injection pressure due to the lower solubility and a larger portion of the injected CO_2 played a major role in displacement at the same injection rate. With the growth of the injection pressure, the ultimate ORF at the terminal 2.0 PV increased due to the stronger interaction ability between the CO_2 and the crude oil.

Figure 7 shows the oil recovery, asphaltene content and viscosity of the produced oil for five coreflood tests at different injection pressures. The oil recovery factor increased significantly with the increasing injection pressure until reaching the MMP = 17.02 MPa. This is because the viscosity of the crude oil and the InterFacial Tension (IFT) between the crude oil and CO_2 decreased at higher injection pressure [11]. In addition, it can been seen from Figure 7 that the viscosity of the produced oil decreased from 10.18 mPa s to 3.72 mPa s when the injection pressure increased from 9.1 MPa to 22.1 MPa. And, the asphaltene content of the produced oil decreased from 0.78 wt% to 0.58 wt% as the injection pressure increasing from 9.1 MPa to 16.2 MPa, while the asphaltent content barely changed when the injection was higher than the MMP (Fig. 7). The aphaltene content of the original oil is 0.94 wt%, which is always higher than that of the produced oil. This result means there is asphaltene precipitation left in the core during CO_2 coreflood process. The higher is the asphaltene content of the produced oil, the more is asphaltene left in the core sample.

3.4 Effect of asphaltene precipitation during CO_2 flooding

3.4.1 *The effect of asphaltene precipitation on permeability*

In this study, the percentage of permeability reduction was obtained by comparing the gas permeability of the core before and after CO_2 flooding, as in the following equation:

$$Pr = \frac{K_{gb} - K_{ga}}{K_{gb}}, \tag{7}$$

Pr : the permeability reduction percentage of the core sample, %;
K_{gb}: the gas permeability of the core sample before CO_2 flooding, mD;
K_{ga}: the gas permeability of the core sample after CO_2 flooding, mD.

Figure 8 plots the percentage of permeability reduction of the core samples and asphaltene content of the produced oil at different injection pressures. The asphaltene left in the pores could be inferred from the content of the produced oil. If the asphaltene content of the produced oil was higher, it indicated that there was less asphaltene precipitation in the pores of core sample. It can be seen from Figure 8 that the asphaltene content of the produced oil decreased with the increased injection pressure. But, when the injection pressure approached the MMP, the asphaltene content was almost unchanged.

Similarly, the percentage of permeability reduction significantly increased from 2.4% to 7.41% as the injection pressure increased in the immiscible stage from 9.1 MPa to 16.2 MPa. When the injection pressure reached the MMP, the percentage of permeability reduction still increased with the injection pressure increasing, but changed slowly compared with that in the immiscible stage.

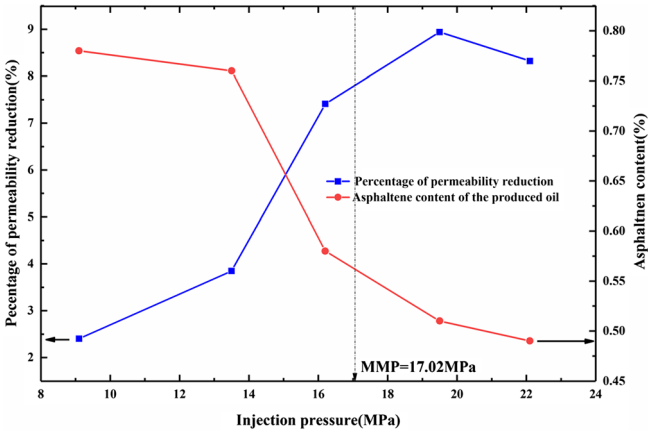

Fig. 8. The percentage of permeability reduction of the core samples and asphaltene content of the produced oil at different injection pressures.

The results were consisted with the asphaltene content of the produced oil at different injection pressures. As a result, more asphaltene would precipitate and block the pores with increasing pressure until the injection pressure reached the MMP.

3.4.2 The effect of asphaltene precipitation on pore structure

As mentioned in the coreflood experimental procedure, the T_2 spectrum for the initial water-saturated cores and the T_2 spectrum for the water-saturated cores after CO_2 flooding were measured and compared. Figure 9 illustrates the T_2 spectrum distributions for cores 2–1, 2–3 and 2–5. The NMR spectrum of the core samples was typical bimodal distribution as shown in Figures 3 and 9. It could be seen from Figure 9 that the T_2 spectrum measured for the water-saturated core after CO_2 flooding moved a slightly lower position compared to that measured for the initial water-saturated core. Because the petroleum ether was used to clean the cores after CO_2 flooding and asphaltene cannot dissolve in the petroleum ether [12]. The reduced amplitude of the T_2 spectrum indicated the pores were clogged due to the asphaltene precipitation and deposition, which could not be saturated with water. The initial water saturated in the pores and the water saturated in the pores after CO_2 flooding is defined as S_{wb} and S_{wa} respectively, the severity of formation damage due to asphaltene precipitation could be calculated as follows:

$$D_w = \frac{S_{wb} - S_{wa}}{S_{wb}} \times 100\%, \quad (8)$$

D_w: the severity of formation damage due to asphaltene precipitation;
S_{wb}: the summation of the water saturated in the pores of the core before CO_2 flooding;

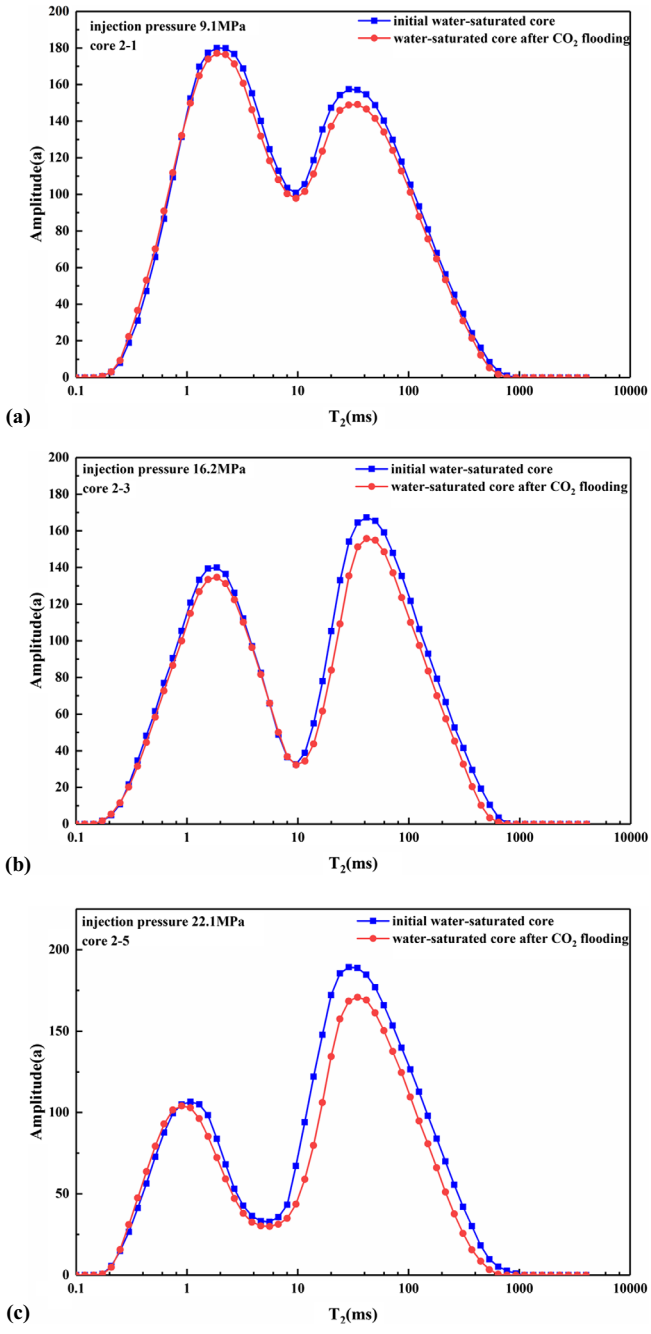

Fig. 9. Comparison of T_2 spectrum for the initial water-saturated cores and for the water-saturated cores after CO_2 flooding and cleaning.

S_{wa}: the summation of the water saturated in the pores of the core after CO_2 flooding.

The severity of formation damage due to asphaltene precipitation of the cores 2–1, 2–3 and 2–5 was 3.67%, 8.20% and 13.75%, respectively. And the permeability reduction corresponding to the three cores was 2.4%, 7.41%, 8.32%. The severity of formation damage due to asphaltene precipitation increased as the injection pressure

Table 4. T_2 spectrum distribution obtained from NMR tests for the three core samples.

Core no.	Injection condition		T_2 distribution (%)			
			0.1–1 ms	1–10 ms	10–100 ms	100–1000 ms
2–1	9.1 MPa	Before CO_2 flooding	14.07	38.50	35.87	11.55
		After CO_2 flooding	15.19	38.56	35.19	11.06
		Difference	+1.12	+0.06	−0.68	−0.49
2–3	16.2 MPa	Before CO_2 flooding	11.84	32.97	39.00	16.19
		After CO_2 flooding	12.22	34.93	37.84	15.01
		Difference	+0.38	+1.96	−1.16	−1.18
2–5	22.1 MPa	Before CO_2 flooding	13.12	20.71	49.32	16.85
		After CO_2 flooding	16.13	20.97	48.18	14.72
		Difference	+3.01	+0.27	−1.15	−2.13

increased. Moreover, the pore distribution influenced by asphaltene precipitation expanded in the miscible stage (Fig. 9). Because CO_2 could expand sweep area and enter smaller pores to interact with the crude oil at higher injection pressure.

The amplitude variation of the micro (0.1–1 ms) and small pores (1–10 ms) was smaller than the amplitude variation of the medium (10–100 ms) and large pores (100–1000 ms). That indicated that the asphaltene precipitation had a greater influence on the medium and large pores. The interaction between the CO_2 and crude oil in the medium and large pores was sufficient, so that the asphaltene precipitation in the medium and large pores was more serious than micro and small pores (Fig. 9). When the asphaltene precipitated in the tight sandstone reservoirs, the larger particles could block up the pore throat directly [33], while the smaller ones could cause an obstacle or blockage in the pore or pore throat [8]. On the other hand, although part of the micro and small cores were blocked by precipitated asphaltene particles, the medium and large pore radius decreased due to asphaltene precipitation. The medium and large pores transformed into the micro and small pores. Thus, the amplitude of micro and small cores changed little.

Table 4 shows the T_2 spectrum distribution which corresponds to pore distribution for the three core samples. The proportion of medium and large pores of the cores after CO_2 flooding decreased while the proportion of micro and small pores increased, compared to the initial water-saturated cores. The pore distribution of tight cores after CO_2 flooding overall changed to the direction of pore radius reduction after CO_2 flooding. Moreover, the proportion changed more greatly at higher injection pressure.

3.4.3 The effect of asphaltene precipitation on wettability

In consistent with the variation of T_2 spectrum in Figure 9 due to the asphaltene precipitation, the T_2 spectrum measured for oil saturated core after CO_2 flooding also deviated slightly lower from that for initial oil-saturated core, as shown in Figure 10. The amount of saturated oil decreased more in medium and large pores (10–1000 ms) than in micro and small pores (0.1–10 ms), as well. However, compared with the difference between the initial water-saturated cores and the water-saturated cores after CO_2 flooding (Fig. 9), the difference between the initial oil saturated in pores and the oil saturated in the pores after CO_2 flooding is smaller (Fig. 10).

S_{ob} and S_{oa} respectively stands for the initial oil saturated in the pores and the oil saturated in the pores after CO_2 flooding. The relative variation of the T_2 spectrum in Figure 10 due to asphaltene precipitation could be calculated, as follows:

$$D_o = \frac{S_{ob} - S_{oa}}{S_{wb}} \times 100\% \tag{9}$$

$$I_{WA} = D_w - D_o, \tag{10}$$

D_o: the relative variation of the T_2 spectrum due to asphaltene precipitation;
S_{ob}: the summation of the oil saturated in the pores of the core before CO_2 flooding;
S_{oa}: the summation of the oil saturated in the pores of the core after CO_2 flooding;
I_{WA}: the wettability alteration index of the core before and after CO_2 flooding.

The pores occupied by asphaltene deposition are constant, so that the D_o should have been same as the D_w, theoretically. However, the D_o is less than the D_w, which means that some pores could be saturated more oil than water after the CO_2 flooding compared with that before CO_2 flooding, relatively. The wettability alteration was assumed to occur due to asphaltene precipitation. The wettability of the rock after CO_2 flooding altered to the oil-wet direction. The index of the wettability alteration can be represented by I_{WA}. When the I_{WA} is zero, there is no wettability

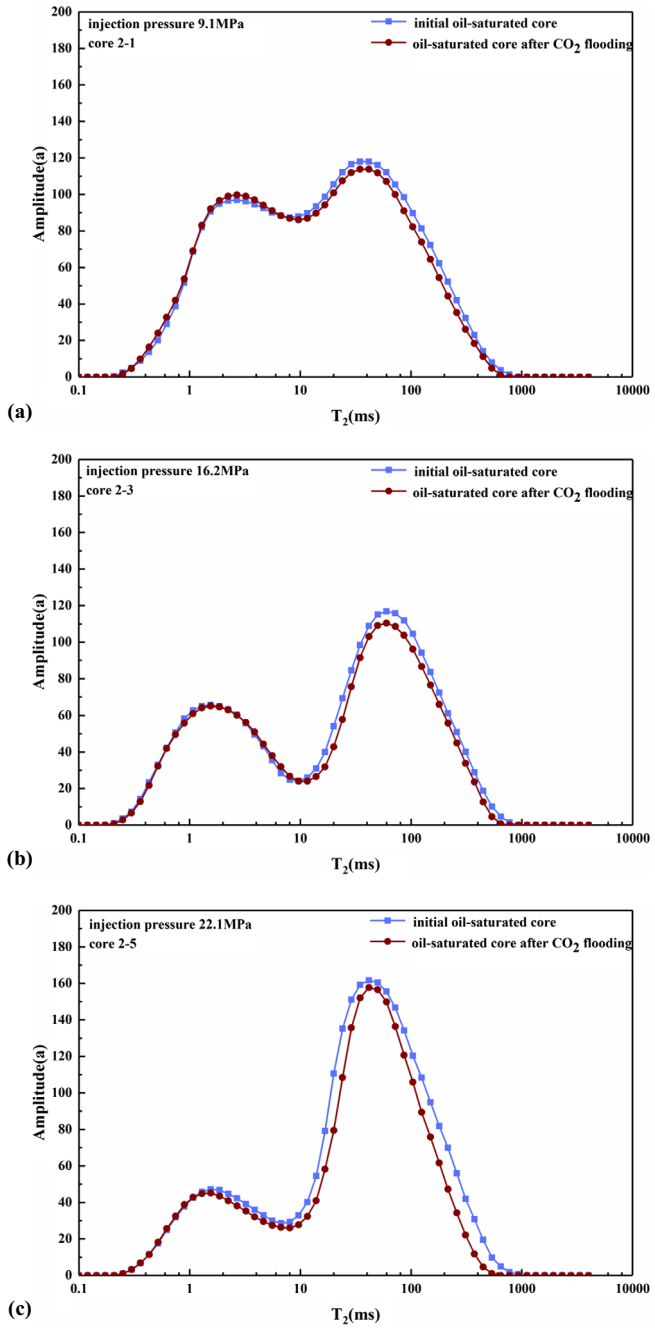

Fig. 10. Comparison of T_2 spectrum for the initial oil-saturated cores and for the oil-saturated cores after CO_2 flooding and cleaning.

alteration. When the I_{WA} is higher than zero, the wettability changes to oil-wet direction and the larger I_{WA} means stronger oil-wet alteration. The I_{WA} of the core samples after CO_2 flooding at different pressures are presented in Table 5. Therefore, the reduction of water permeability was caused by pore clogging and wettability alteration. If the CO_2-EOR technique is applied, it is necessary to injection chemical inhibitor into the reservoir to reduce the risk of asphaltene precipitation.

Table 5. The relative variation of the T_2 spectrum in condition of water saturation and oil saturation respectively.

Core no	Injection pressure (MPa)	D_w (%)	D_o (%)	I_{WA} (%)
2–1	9.1	3.67	1.96	1.70
2–3	16.2	8.20	4.12	4.08
2–5	22.1	13.75	9.79	3.97

4 Conclusion

In this paper, five CO_2 coreflood tests were conducted at immiscible, near-miscible and miscible conditions. For each test, the ORF, the viscosity and the asphaltene contents of the produced oil were analyzed. Then, the distribution of asphaltene precipitation in the pores and wettability alteration was quantitatively evaluated.

It is found that, the extraction effect of the CO_2 played a more dominant role in the CO_2-EOR process with higher injection pressure. So that more light components are extracted and recovered by the CO_2 and more heavy components including asphaltene were left in the core at higher injection pressure. And, the asphaltene precipitated in the core had little increase in the CO_2 miscible flooding stage.

The severity of formation damage influenced by asphaltene precipitation increased with the increasing of injection pressure. And, the asphaltene precipitation had a greater influence on the medium and large pores due to the sufficient interaction between the CO_2 and crude oil. Furthermore, the asphaltene precipitation not only caused pore clogging, but also induced rock wettability alteration towards oil-wet direction. If the CO_2-EOR technique is applied, it is necessary to injection chemical inhibitor into the reservoir to reduce the risk of asphaltene precipitation.

Acknowledgments. We thank the *State Key Lab of Oil and Gas Resources and Engineering* at the *China University of Petroleum-Beijing (CUPB).* This research is supported by the National Science and Technology Major Project of the *Ministry of Science and Technology of China* (Grant 2016ZX05016-006).

References

1 Holm L.W., Josendal V.A. (1974) Mechanisms of oil displacement by carbon dioxide, *J. Pet. Technol.* **26**, 12, 1427–1438.
2 Rahimi V., Bidarigh M., Bahrami P. (2017) Experimental study and performance investigation of miscible water-alternating-CO_2 flooding for enhancing oil recovery in the Sarvak formation, *Oil Gas Sci. Technol. - Rev. IFP Energies nouvelles* **72**, 35.
3 Ko S.C.M., Stanton P.M., Stephenson D.J. (1985) Tertiary recovery potential of CO_2 flooding in Joffre Viking pool, Alberta, *J. Can. Pet. Technol.* **24**, 1, 36–43.
4 Mungan N. (1966) Interfacial effects in immiscible liquid-liquid displacement in porous media, *Soc. Pet. Eng. J.* **6**, 3, 247–253.

5 Sarma H.K. (2003) Can we ignore asphaltene in a gas injection project for light-oils? *SPE International Improved Oil Recovery Conference in Asia Pacific*, 20–21 October, Kuala Lumpur, Malaysia, Society of Petroleum Engineers.

6 Tabzar A., Fathinasab M., Salehi A., Bahrami B., Mohammadi A.H. (2018) Multiphase flow modeling of asphaltene precipitation and deposition, *Oil Gas Sci. Technol. - Rev. IFP Energies nouvelles* **73**, 51.

7 Abedini A., Ashoori S., Torabi F. (2011) Reversibility of asphaltene precipitation in porous and non-porous media, *Fluid Phase Eq.* **308**, 1–2, 129–134.

8 Hu Y.F., Li S., Liu N., Chu Y.P., Park S.J., Ali Mansoori G., Guo T.M. (2004) Measurement and corresponding states modeling of asphaltene precipitation in Jilin reservoir oils, *J. Pet. Sci. Eng.* **41**, 1–3, 169–182.

9 Hamouda A.A., Chukwudeme E.A., Mirza D. (2009) Investigating the effect of CO_2 flooding on asphaltenic oil recovery and reservoir wettability, *Energy Fuels* **23**, 2, 1118–1127.

10 Wang C., Li T., Gao H., Zhaoa J., Li H.A. (2017) Effect of asphaltene precipitation on CO_2-flooding performance in low-permeability sandstones: A nuclear magnetic resonance study, *RSC Adv.* **7**, 61, 38367–38376.

11 Cao M., Gu Y. (2013) Oil recovery mechanisms and asphaltene precipitation phenomenon in immiscible and miscible CO_2, flooding processes, *Fuel* **109**, 157–166.

12 Wang Z., Yang S., Lei H., Yang M., Li L., Yang S. (2017) Oil recovery performance and permeability reduction mechanisms in miscible CO_2 water-alternative-gas (WAG) injection after continuous CO_2 injection: An experimental investigation and modeling approach, *J. Pet. Sci. Eng.* **150**, 376–385.

13 Amroun H., Tiab D. (2001) Alteration of reservoir wettability due to asphaltene deposition in Rhourd-Nouss Sud Est Field, Algeria, *SPE Rocky Mountain Petroleum Technology Conference*, Society of Petroleum Engineers.

14 Escrochi M., Nabipour M., Ayatollahi S.S., Mehranbod N. (2008) Wettability alteration at elevated temperatures: The consequences of asphaltene precipitation, *SPE International Symposium and Exhibition on Formation Damage Control*, Society of Petroleum Engineers.

15 Uetani T. (2014) Wettability alteration by asphaltene deposition: A field example, *Abu Dhabi International Petroleum Exhibition and Conference*, Society of Petroleum Engineers.

16 Abedini A., Torabi F. (2014) Oil recovery performance of immiscible and miscible CO_2 huff-and-puff processes, *Energy Fuels* **28**, 2, 774–784.

17 Wang X., Gu Y. (2011) Oil recovery and permeability reduction of a tight sandstone reservoir in immiscible and miscible CO_2 flooding processes, *Ind. Eng. Chem. Res.* **50**, 4, 2388–2399.

18 Srivastava R.K., Huang S.S., Dong M. (1999) Asphaltene deposition during CO_2 flooding, *SPE Prod. Facil.* **14**, 04, 235–245.

19 Song Z., Zhu W., Wang X., Guo S. (2018) 2-D pore-scale experimental investigations of asphaltene deposition and heavy oil recovery by CO_2 flooding, *Energy Fuels* **32**, 3194–3201.

20 Fleury M., Deflandre F. (2003) Quantitative evaluation of porous media wettability using NMR relaxometry, *Magn. Reson. Imag.* **21**, 3–4, 385–387.

21 Looyestijn W.J., Hofman J. (2006) Wettability-index determination by nuclear magnetic resonance, *SPE Reserv. Evalu. Eng.* **9**, 02, 146–153.

22 Shikhov I., Li R., Arns C.H. (2018) Relaxation and relaxation exchange NMR to characterise asphaltene adsorption and wettability dynamics in siliceous systems, *Fuel* **220**, 692–705.

23 Amott E. (1959) Observations relating to the wettability of porous rock, *Trans. AIME* **216**, 156–162.

24 ASTMD2007-03 (2007) *Standard test method for characteristic groups in rubber extender and processing oils and other petroleum-derived oils by the clay-gel absorption chromatographic method*, ASTM International, West Conshohocken, PA.

25 Sheu E.Y. (2002) Petroleum asphaltene properties, characterization, and issues, *Energy Fuels* **16**, 1, 74–82.

26 Coates G.R., Xiao L., Prammer M.G. (1999) *NMR logging: Principles and applications*, Halliburton Energy Services, Houston, pp. 8–33.

27 Loren J.D., Robinson J.D. (1970) Relations between pore size fluid and matrix properties, and NML measurements, *Soc. Pet. Eng. J.* **10**, 3, 268–278.

28 Megawati M., Madland M.V., Hiorth A. (2012) Probing pore characteristics of deformed chalk by NMR relaxation, *J. Pet. Sci. Eng.* **100**, 123–130.

29 Yu Z., Liu L., Yang S., Li S., Yang Y. (2012) An experimental study of CO_2–brine–rock interaction at in situ pressure–temperature reservoir conditions, *Chem. Geol.* **326**, 88–101.

30 Mohamed I.M., Nasr-El-Din H.A. (2012) Formation damage due to CO_2 sequestration in deep saline carbonate aquifers, *SPE International Symposium and Exhibition on Formation Damage Control*, Society of Petroleum Engineers.

31 Fischer S., Liebscher A., Wandrey M., the CO_2 SINK Group (2010) CO_2–brine–rock interaction – first results of long-term exposure experiments at in situ P-T conditions of the Ketzin CO_2 reservoir, *Chemie Erde* **70**, 155–164.

32 Yu M., Liu L., Yang S., Yu Z., Li S., Yang Y., Shi X. (2016) Experimental identification of CO_2–oil–brine–rock interactions: Implications for CO_2 sequestration after termination of a CO_2-EOR project, *Appl. Geochem.* **75**, 137–151.

33 Mendoza de la Cruz J.L., Argüelles-Vivas F.J., Matías-Pérez V., Durán-Valencia C.A., López-Ramírez S. (2009) Asphaltene-induced precipitation and deposition during pressure depletion on a porous medium: An experimental investigation and modeling approach, *Energy Fuels* **23**, 11, 5611–5625.